Geosci. Instrum. Method. Data Syst. Discuss., 4, 491–513, 2014
www.geosci-instrum-method-data-syst-discuss.net/4/491/2014/
doi:10.5194/gid-4-491-2014

Geoscientific Instrumentation Methods and Data Systems Discussions
Open Access

Image GeoRectification And Feature Tracking toolbox: ImGRAFT

A. Messerli[1,2] **and A. Grinsted**[1]

[1]Centre for Ice and Climate, Niels Bohr Institute, University of Copenhagen, Juliane Maries Vej 30, 2100 Copenhagen Ø, Denmark
[2]Section for Glaciers, Snow and Ice, Hydrology Department, Norwegian Water Resources and Energy Directorate, P.O. Box 5091 Majorstua, 0301 Oslo, Norway

Received: 31 July 2014 – Accepted: 15 August 2014 – Published: 25 August 2014

Correspondence to: A. Messerli (messerli@nbi.ku.dk)

Published by Copernicus Publications on behalf of the European Geosciences Union.

Abstract

The use of time-lapse camera systems is becoming an increasingly popular method for data acquisition. The camera setup is often cost-effective and simple, allowing for a large amount of data to be accumulated over a variety of environments for relatively minimal effort. The acquired data can, with the correct post-processing, result in a wide range of useful quantitative and qualitative information in remote and dangerous areas. The post-processing requires a significant amount of steps to transform images into meaningful and comparable data, such as velocity data. To the best of our knowledge at present a complete, openly available package that encompasses georeferencing, georectification and feature tracking of terrestrial, oblique images is still absent. This study presents a complete, yet adaptable, open-source package developed in MATLAB, that addresses and combines each of these post-processing steps into one complete suite in the form of an "Image GeoRectification and Feature Tracking" (ImGRAFT: http://imgraft.glaciology.net) toolbox. The toolbox, can also independently produce other useful outputs, such as viewsheds, georectified and orthorectified images. ImGRAFT is primarily focused on terrestrial oblique images, for which there are currently limited post-processing options available. In this study we illustrate ImGRAFT for glaciological applications on a small outlet glacier Engabreen, Norway.

1 Introduction

The use of terrestrial photography as a means of understanding spatio-temporal landscape evolution and change is not a new concept. It spans a vast range of disciplines including disaster monitoring (Mulsow et al., 2013), glacier motion (Flotron, 1973; Harrison et al., 1986; Ahn and Box, 2010), mountain ecosystem understanding (Aschenwald et al., 2001), hydrological monitoring (Parajka et al., 2012; Danielson and Sharp, 2013) and snow monitoring (Smith Jr. et al., 2003; Corripio, 2004; Härer et al., 2013). It is a cheap, cost effective, simple method that allows the researcher to obtain

GID
4, 491–513, 2014

a vast array of information about their study site. Today more and more disciplines are discovering the immense power of terrestrial photography for both qualitative and quantitative applications due to the high repeat imaging capacity. The quantitative aspect relies heavily on the ability of the image to be georectified to a meaningful coordinate system. In order to achieve this, Ground Control Points (GCPs) are needed and a good high resolution Digital Elevation Model (DEM) often makes this process more successful. The conversion from image coordinates to real-world coordinates gives each image pixel a true estimate of the space they represent. In its simplest form this might be the actual scale each pixel represents in metres. The more complex rectification includes a full registration of the image to an established coordinate system through georeferencing.

Examples of quantitative data are velocity fields of glaciers and other mass movement, such as a landslide or rock glacier (Kääb and Vollmer, 2000; Kääb, 2002; Debella-Gilo and Kääb, 2011). Here we shall focus on velocity measurements however, in addition to velocity, cameras provide other additional supporting information about the field site that is otherwise only be obtained from prolonged field campaigns. For example, the exact timing of the first snowfall and at which elevation. This data can support and validate other records from the area such as precipitation gauges. In some cases time-lapse imagery has been used to validate seismic data to detect large calving events at large outlet glaciers (Walter et al., 2010).

In this paper we present the new Image GeoRectification and Feature Tracking (ImGRAFT) toolbox. We perform a full georectification of the images using a own newly developed processing chain. Once rectified images are used to produce velocity fields at the glacier test site Engabreen. The ice displacement is determined using a cross-correlation feature tracking algorithm. Previous studies stretching back to the 1970s have also used time-lapse imagery as a means of monitoring glacial flow (e.g. Flotron, 1973; Harrison et al., 1986). These studies used various approaches to achieve the same result of obtaining ice flow estimates by tracking either existing features on the ice such as crevasses (Harrison et al., 1992; Evans, 2000; Ahn and Box, 2010) or specific

GID
4, 491–513, 2014

targets placed on the glacier such as in Harrison et al. (1986). Here we present our method as an open source "toolbox" for georectification and feature tracking terrestrial images. This toolbox adds to the growing base of feature tracking and rectification software and toolboxes. A full working example, the source code and additional information can be found in the examples section of the toolbox website (Messerli and Grinsted, 2014).

2 Motivation

The most successful methods usually focus on either feature tracking or georectification (Corripio, 2004; Härer et al., 2013). To date the most commonly used publicly available feature tracking software are IMCORR (NSIDC) and COSI-Corr (CALTECH) software. Both IMCORR from the US National Snow and Ice Data Center (NSIDC), Boulder, CO and COSI-Corr from California Institute of Technology (CalTech), Pasadena, CA, are optimised for use with aerial and satellite imagery where the rectification process is fairly straight forward compared to that of an oblique terrestrial image, as in our case. Photogeoref developed by Corripio (2004) and the recent release of PRACTICE (Photo Rectifcation And ClassificaTIon SoftwarE) based on Photogeoref which has been further improved and developed by Härer et al. (2013), focus mainly on the georectification of oblique images. During the testing stages we found difficulties with automation due to the use of separate existing georectification and feature tracking tools. Additionally a workflow was needed that was able to deal with camera motion and lens distortion efficiently. Another concern was that traditional image registration as a pre processing step can introduce loss of image quality and detail through resampling. As a result we were prompted to develop a new toolbox that met all the requirements including the georectification and feature tracking processes all to be contained within one MATLAB package. Batch processing of the entire workflow is easily achieved through a case specific custom script, a feature not often available in other image feature tracking methods.

GID
4, 491–513, 2014

3 Field set up and data

The test site for ImGRAFT is located at Engabreen in northern Norway (Fig. 1). Engabreen is a small Arctic valley glacier and outlet of the large Svartisen Ice Cap. Engabreen has a large icefall located at approximately 850 m a.s.l.. An icefall is a steep area of the glacier where there is high ice flow and as a result extensional flow leading to extensive development of large crevasses and unstable ice blocks known as *séracs* (Benn and Evans, 2010). In previous years attempts have been made to instrument the icefall however due to the nature of the moderate flow ($> 300\,\mathrm{m\,year^{-1}}$) and the extensive crevassing the longevity of any instrument in this region is generally short-lived.

Our camera set-up in the field consisted of one Canon Rebel T3 (1100D) single-lens reflex camera controlled by a *Harbortronics DigiSnap* intervalometer set up (https://www.harbortronics.com/Products/TimeLapsePackage/). The camera was programmed to take seven pictures per day at three hour intervals at the following times: 05:04, 08:04, 11:04, 14:04, 17:04, 20:04 and 23:04 CEST. During our six month monitoring period we experienced a drift in the intervalometer of approximately five seconds over six months. We used a *Sigma* prime lens with a focal length of 30 mm. We mounted our camera in a fibreglass, water tight enclosure on a on a solid metal frame structure that was concreted in to the ground. The camera system was powered by an 11.1 Volt 9000 mAh lithium polymer battery pack and supported by a 5 Watt solar panel. The camera was positioned on the eastern margin of the glacier, at about 770 m elevation on the valley side overlooking an icefall (Fig. 4a). The average height of the surface of the glacier measured was approximately 550 m a.s.l., so the camera was approximately 220 m above the average surface and 120 m above the highest point we measured. The look angle of the camera was approximately 13°. A key component of this process is that the DEM used in the georectification is as recent as possible and of as high resolution as possible. Fortunately in this case a high resolution DEM was produced from an airborne laser scan which took place during the monitoring period on the 25 August 2013. This is extremely useful for georectifying the time lapse images as

GID
4, 491–513, 2014

both a DEM and at least one of the time lapse images from the exact same time exist. This means that we have an absolute surface that we were able to use to rectify our images. In addition to this, a high resolution (10 cm) orthophoto of the entire area of the laser scan was taken from a camera mounted on board the plane. This combination of the DEM and orthophoto made the selection of additional GCPs easier and we were able to select many visible features in the camera field of view (FOV) that significantly aided the subsequent georectification of our images. We overlaid the orthophoto onto the DEM and picked out the features for our GCPs manually. Features included; the entrance to a subterranean tunnel on the western valley side, spray painted boulders, other large distinct boulders and the edges of dominant, persistent snow patches in gulleys. In addition to the rock features we were also able to use the crevasses as GCPs as a result of the exact overlap of the image and DEM acquisition. A small number of GCPs were measured using a global positioning system (GPS), these include the tunnel and the spray painted boulder.

3.1 Image preparation

Firstly we converted all collected images from RAW to tiff format using dcraw (Coffin, 2009). We chose a linear gamma curve in the conversion to preserve the dynamic range of the bright ice. We manually inspected the images to determine if they were suitable for feature tracking purposes or not, and removed all images that were deemed to be unusable. These included images that were taken at night and those where either all or a significant portion of the glacier were obscured by cloud or fog. Images where there appeared to be heavy rainfall were also removed as the raindrops themselves lead to extra distortion as they settle on the camera window. To allow for a better comparison we also selected image pairs at the same time of day as the sun illumination was more consistent over the glacier and valley. This also means that the shadowing around large crevasse features is similar between each image (Ahn and Box, 2010). Like with any time lapse camera set up, trying to reduce the amount of movement of the camera is vital. Even though the camera was mounted on a solid structure it is

GID
4, 491–513, 2014

almost impossible to avoid some form of camera motion. This can be due to strong winds, thermal expansion of the camera enclosure or of the mounting platform and human interference, for example when changing SD memory cards. This motion introduces errors and need to be corrected for, as does the distortion around the edge of the image as a result of the curvature of the glass in the lens. We address these issues in the method section.

The images that were collected in early spring when snowfall was still regular presented another problem: a lack of rock features for detecting camera motion, a lack of distinct glacier features (as they are covered by snow) and finally a rapidly changing surface. Lastly the surface features change rapidly from one day to the next, either through new snowfall or as we saw later on rapid melting.

3.2 DEM preparation

The DEM is a fundamental input in our method (Fig. 2) and needs to be prepared correctly for our purpose. We initially used a 1 m high resolution DEM, however on inspection of the results we identified some complications. The complications arose as large persistent features such as crevasses and *séracs* moved down glacier over time. As a result it implies that after a day the DEM that encompasses the high resolution crevasses detail no longer represents the ice in the images. This is because the high peaks and low troughs of these crevasses are now downstream. For example, points that correspond to a peak of a crevasse in the image could be a trough in the DEM and vice versa due to the motion of the glacier. To avoid this problem further we decided to "fill" our crevasses in the DEM so that we removed the large local variability in the glacier surface caused by these large crevasses and *séracs* to achieve a smoother, more consistent surface.

We fill the crevasses using image filtering techniques. First we smooth the DEM (z) with a Gaussian spatial filter (S_g), which results in a DEM which lies lower than the original. The deviation between the smoothed DEM and the original is passed through a non-linear function (exp) and spatially smoothed with a disk filter (S_d). This strongly

GID
4, 491–513, 2014

weighs positive deviations from the smoothed DEM, i.e. crevasse tops. The final DEM (z_{filled}) is the smoothed DEM plus the upper surface DEM.

$$z_{\text{filled}} = a \log\left(S_{\text{d}}\left(\exp\frac{z - S_{\text{g}}(z)}{a}\right)\right) + S_{\text{g}}(z),$$

where a is the weighting constant and in this case equal to 1 m. We apply a final smoothing (S_{g}) to reduce the stepped nature of z_{filled}. The characteristic length scale of the smoothing operators has been chosen to bridge the largest crevasses.

We are fortunate to have obtained a DEM on the 25 August 2013 between 10:20 and 11:13 CEST, and an image was taken on the same day at 11:04 CEST. We are therefore able to fully rectify our image according to the DEM. This full rectification however is only correct during that time on that day. Henceforth this image will be called *Master image* (Fig. 2). In all other images the ice surface is incorrect. This is due to the evolution of the ice surface as a result of melting. On an ice surface where melting occurs throughout the ablation season, it is important to consider this effect on the accuracy of the results. At Engabreen we experience a significant surface lowering on the order of 10 m on the lower tongue during a single melt season. This demonstrates the need for a lowering/raising function to be applied to the ice surface. We derive the elevation change factor from direct mass balance measurements taken at the glacier at monthly intervals at elevations 350 m above the viewshed and 200 m below the viewshed.

4 Method

We present the major steps in the processing chain illustrated in Fig. 2. We focus in more detail on the unique ImGRAFT features and provide a short overview of the standard processes. Further information about the practical aspects of ImGRAFT along with a full working example can be found on the toolbox website (Messerli and Grinsted, 2014). This includes the link to the source code and a basic manual.

GID
4, 491–513, 2014

4.1 Distortion and camera determination

For each image we have a corresponding model camera which accounts for any camera motion. We determine the camera view parameters for the master image from GCPs. The view direction, focal lengths, and lens distortion model are optimised to minimise the square projection error using a modified Levenberg-Marquardt algorithm (Fletcher, 1971). The model camera formulation has a close correspondence to that of OpenCV (Bradski, 2000) which is loosely based on Claus and Fitzgibbon (2005). This produces a master camera which we use to reference all other model cameras to. Our method differs slightly from other similar methods, as we adopt a different approach to dealing with camera motion. Camera motion, as discussed previously, caused by a variety of uncontrollable factors that subsequently lead to an offset between image pairs. The main motion experienced is the rotation about the vertical (yaw), as the camera was mounted on a round pole. However we experience rotation about all three axes (compass direction/yaw, inclination/pitch, horizon-tilt/roll). We firstly need to determine the offset. This is done by tracking stable rock features on both the near and far valley sides. From this we able to determine the amount and type of motion. We then use this information to "update" the view direction of the camera model. In practice we project the master image pixel coordinates to the new model camera and optimize the camera view by minimising the reprojection error (see Messerli and Grinsted, 2014). Instead of correcting the image we correct the camera orientation based on the offset. This is advantageous since we only save a text file rather than a large corrected image, but also avoid compromising image quality that can occur from cropping, rotating and re-saving.

4.2 Georectification

Oblique imagery lacks crucial spatial information needed to extract useful quantitative distance (dimension) information as the image is a 2-D representation of a 3-D landscape (Corripio, 2004; Härer et al., 2013) Georectification is the process whereby we

GID
4, 491–513, 2014

assign a 3-D real world coordinate to the corresponding pixel in the 2-D image. The model camera directly allows us to calculate the 2-D pixel coordinates of any 3-D real world coordinates. However, we are interested in the 3-D coordinates of features in the image. I.e. we want to make an "inverse" projection from 2-D pixel coordinates to 3-D coordinates, constrained to the visible part of the DEM. In ImGRAFT we project the visible part of the DEM to 2-D camera view coordinates, and use standard interpolation techniques to obtain 3-D coordinates for any image pixel.

4.3 Feature matching

ImGRAFT tracks features between images, *image A* and *image B* (Figs. 2 and 3) by a process called template matching. *Image A* refers to the template image and *image B* refers to the search image. The initial version of ImGRAFT uses normalised cross correlation (NCC) as a measure of feature similarity, which generally performs well (Heid and Kääb, 2012) but other measures such as phase correlation and optical flow analysis have been suggested in the literature (Ahn and Box, 2010; Ahn and Howat, 2011; Heid and Kääb, 2012; Vogel et al., 2012). ImGRAFT uses the same NCC template matching algorithm when tracking camera motion and ice flow. This particular method is sensitive to changing light conditions around the feature and to and reduce this effect we only choose image pairs where illumination is similar, i.e. we only use image pairs taken at the same time of day. For that reason we also generate secondary master images for varying image conditions based on, illumination and snow coverage, in addition to the "Master image". One way to reduce false matches is by reducing the size of the search window and centring it on a prior estimate of the location in the second image in the image pair, *image B* (Fig. 2). In our case the prior guess is based on the centre coordinate of the template in *image A*, reprojected to the view from camera B. This prior guess accounts for camera motion, but it could be improved with a background ice flow estimate.

GID
4, 491–513, 2014

We obtain subpixel displacements by bi-cubic intensity interpolation as used in Debella-Gilo and Kääb (2011), followed by local weighing of the NCC peak (3-by-3 pixel) neighbourhood.

It is common to track a regular grid based on pixel coordinates, however due to the geometry of the glacier this corresponds to an irregular grid in 3-D space, often characterised by gaps in the velocity field. This is because the grid is not fixed in space but rather image specific as a result of camera motion. Instead we use a static, regular (25 m) geographic grid (Fig. 3) to track features on the ice thereby consistently tracking the same coordinate through time. This allows for a better comparison between velocity fields from different time periods.

4.4 Velocity calculation

The feature tracking returns the pixel coordinates of the feature in the image pair (*image A* and *image B*). The corresponding 3-D world coordinates are obtained using the inverse projection of the model camera. The velocities can then be calculated from the change in geographic location. Having very oblique angles can amplify errors along the look vector. In this case it can be beneficial to only look at the velocity component along the flow direction (i.e local slope direction or along centreline). The velocity maps presented in Fig. 4 are a raw data display of the full magnitude of the velocity and are not projected along the slope direction or along centreline.

5 Quality control

Subsets of the velocity field were extracted from regions of slow, high and medium flow. The slow flow regions are around the margins was one obvious quality control area where one expects highest friction on the valley sides. We assume that small errors will propagate to areas furthest away from the camera, and therefore we begin our quality control checks here. If the margin areas indicate high velocities, similar to

GID
4, 491–513, 2014

those in the centre of the glacier then it is indicative of an error in our processing chain of that image pair. The mistake is likely to be as a result of the model camera used in the calculation. In order to correct this the "template match rock" stage in the processing chain (Fig. 2) must be re-run to reproduce the offset between stable features. This can then be used to recalculate the camera using "offset to camera" (Fig. 2). If this does not solve the high velocity issue then there may be a problem with the image itself. Light fog and rain can cause problems in the feature tracking of the features in the image leading to false readings. If this problem persists the velocity field is removed.

Error estimation

It is common to estimate the uncertainties in the derived velocity field using an error budget approach (Ahn and Box, 2010). This includes error in registration template matching for both rock and ice, and finally in the transformation from 2-D to 3-D coordinates. In practice the individual terms can be quite challenging to estimate objectively and often ad hoc conservative values are adopted. This has the disadvantage that error estimates can not be used to optimise the individual processing steps, such as template matching algorithm. In our case we attempt to account for all of the accumulated error from each processing step into one final estimate. We use a very simplified but effective empirical method to get an overall estimate of the error in the velocity calculations. We calculate multiple different velocity fields covering effectively the same time period, using independent image pairs (Table 1). The spread in estimates can be considered to be the uncertainty (Table 1). Included in this estimate is the error in template matching, camera registration and 2-D to 3-D transformation. Errors in the DEM would bias all estimates and therefore has to be considered separately for example by Monte Carlo perturbation of the DEM. In our case this is considered small due to the timing of the LiDAR acquisition and thus is not considered.

GID
4, 491–513, 2014

6 Results

ImGRAFT produces consistent velocity fields over the mid icefall section of Engabreen. They match the expected flow pattern of a small alpine glacier, and that of two SAR velocity fields (Unpublished data, Schellenberger, 2014) over the same area. As well as comparing to the SAR maps we also improve the existing surface velocity estimates from Engabreen (Jackson et al., 2005). We significantly improve the temporal coverage due to the high number of images acquired each day. We achieve a dense velocity field at Engabreen albeit over a smaller area than Jackson et al. (2005). The Jackson et al. (2005) study uses a similar photogrammetric approach using IMCORR software, whereby they feature track two aerial images from 2002. They found that the central part of the glacier was moving slower than the margins. Our results and preliminary SAR data indicate that this feature is likely an artefact of the processing due to the long time interval between image acquisitions (> than 20 days). This long interval between images results in features deforming beyond recognition and are thus no longer feasibly trackable. Crevasses tend to generate false matches when the displacement is comparable to the typical crevasse separation distance. The high flow can be separated into two distinct areas; firstly the edge of the upper ice fall flowing into an overdeepening and secondly the ice flowing out of the overdeepening into the lower ice fall as demonstrated by the yellow/orange areas in Fig. 4b.

In addition to calculating velocity estimates for glaciological analysis we calculate velocity fields for distinct time periods in which we expect almost no detectable motion (approximately 2 cm) of the ice. This is done in order to estimate the error within our estimates. Here we offer a little more practical explanation to the previous error Sect. 4.1. Table 1 summarises all of the image pairs used in the error analysis. All image pair IDs that have the suffix *a* consist of pairs taken at 11:04 CEST, and all IDs that have the suffix *b* are image pairs taken at 14:04 CEST. These periods are chosen as they both have high quality images available with similar lighting both at 11:04 and at 14:04 CEST. As discussed earlier for the NCC method, lighting plays a large role in the accuracy of the

GID
4, 491–513, 2014

feature matching as features change significantly according to the sun's position. We selected a small area for more detailed analysis. The subset area (subset 1) we chose, marked with a green box (Fig. 4), appears not to be affected substantially by the sun's position due to the overall geometry of the glacier surface and the small scale local topography. Subset area 1 is the compression zone at the base of the ice fall where the crevasses close and seal, thereby being characterised by a slightly undulating surface with neither high peaks nor troughs as seen in the large ice fall above. It cannot be said that shadows do not modify images from this region, but more that they do not have a significant influence between the hours of 11:04 and 14:04 CEST. This can clearly be seen in the standard deviation plots in (Fig. 4c) where the blue areas fall consistently within the subset 1. Here we compare the offset time period velocity calculations for all image pairs presented in Fig. 1. Figure 4d is the median plot for all the ten time periods together. The final column in Table 1 shows the overall spread in medians between all the time periods. If additional cross image pairs (i.e. 11:04 and 14:04 CEST); which are not shown in Table 1 are compared, the maximum range between all medians for the area subset 1 increases slightly to 5.5 cm day^{-1}. If we only compare the same hour periods in Table 1 the the range is lower at only 5 cm day^{-1}. This is our simple error estimation of the velocity calculation from our feature tracking processing chain. The average velocity for the whole feature tracked area is approximately 60 cm day^{-1} therefore our error estimate of 5 cm day^{-1} equates to a rough error estimate of ±7 % error (or < 10). This error estimate is based on unfiltered data where known mismatch points are included. It is expected that the error will reduce if known mismatches are removed. Some filters were applied to the velocity fields, including correlation coefficient (CC) thresholds set at 0.9 and signal to noise ratio threshold at 2, however we experienced that this removed more positive features than false positive features, therefore we decided to carry out our calculations on unfiltered data.

GID
4, 491–513, 2014

7 Conclusions

We present a flexible newly developed open source Image GeoRectification And Feature Tracking toolbox. ImGRAFT incorporates all the processing steps needed to transform two terrestrial oblique images into a velocity field. ImGRAFT addresses both of these problems in a combined manner assimilated into one toolbox, the source code for which is made freely available.

Our aim is to allow for further algorithm development and improvement through our own efforts and those within the user community. We try to automate as many of the processes as possible but further automation is conceivable. ImGRAFT has the scope to process images taken on lower quality cameras with lower quality lenses as the toolbox incorporates a full distortion model to correct this. This significantly increases the diversity of the toolbox as it accommodates a wide range of image sources and possibilities for feature tracking. ImGRAFT was also tested on Landsat satellite images with very good results, in this instance only the "Template Match" part of the toolbox is required as the satellite images are already fully georeferenced.

ImGRAFT produces consistent velocity fields that require minimal post processing and filtering. A set of standard filters may be applied to the data to remove false matches within the feature tracking algorithm. In the example case (see Messerli and Grinsted, 2014) we apply a signal-to-noise ratio and a CC threshold. It was found that a CC threshold of 0.9 was even too low and removed more positive correlations and as a result we did not filter the results presented in this paper. We propose an empirical approach for error assessment that incorporates the accumulated errors throughout the processing chain. With this approach we do not account for any inaccuracies within the DEM, as these are likely to be negligible in our case as a result of the simultaneous acquisition of the DEM and one of the oblique images on 25 August 2013.

ImGRAFT provides a flexible, adaptable tool to process large volumes of image data to obtain quantitative data in the form of displacement. Whilst we developed ImGRAFT

GID
4, 491–513, 2014

with a focus on glaciological applications, there is nothing to suggest this will not work for other deformation applications.

Acknowledgements. This publication is contribution number 46 of the Nordic Centre of Excellence SVALI, "Stability and Variations of Arctic Land Ice", funded by the Nordic Top-level Research Initiative (TRI). This work was funded by the SVALI project. The camera was purchased by the Centre for Ice and Climate (CIC) and additional funding for fieldwork came from the Scottish Arctic Club and the Anglo-Danish Society. DEM and orthophoto data of Engabreen was provided by the Norwegian Water Resources and Energy Directorate (NVE). The authors would like to thank NVE, especially Miriam Jackson, for logistical and financial support with fieldwork. We would also like to thank Lyndsey Mackay, Heïdi Sevestre and Pierre-Marie Lefeuvre for their support in the field. We also thank A. Kääb for useful discussions in the earlier versions of this study. Also thanks to Nanna Karlsson for reading and offering suggestions on the draft version. Finally we would like to thank T. Schellenberger for providing SAR velocity data over Engabreen, used in the preliminary analysis in this study, but not presented here.

References

Ahn, Y. and Box, J. E.: Instruments and Methods Glacier velocities from time-lapse photos: technique development and first results from the Extreme Ice Survey (EIS) in Greenland, J. Glaciol., 56, 723–734, 2010. 492, 493, 496, 500, 502

Ahn, Y. and Howat, I. M.: Efficient Automated Glacier Surface Velocity Measurement From Repeat Images Using Multi-Image/Multichip and Null Exclusion Feature Tracking, IEEE T. Geosci. Remote, 49, 2838–2846, 2011. 500

Aschenwald, J., Leichter, K., Tasser, E., and Tappeiner, U.: Spatio-temporal landscape analysis in mountainous terrain by means of small format photography: a methodological approach, IEEE T. Geosci. Remote, 39, 885–893, 2001. 492

Benn, D. I. and Evans, D. J. A.: Glaciers and Glaciation, 2nd Edn., Hodder Arnold Publication, Hodder Education, London, 2010. 495

Bradski, G.: OpenCV Library, Dr. Dobb's J. Softw. Tool., 25, 122–125, 2000. 499

Claus, D. and Fitzgibbon, A. W.: A rational function lens distortion model for general cameras, in: IEEE Computer Society Confrence on Computer Vision and Pattern Recognition, Vol. 1, 213–219, 2005. 499

GID

4, 491–513, 2014

Coffin, D.: Decoding raw digital photos in Linux, http://www.cybercom.net/~dcoffin/dcraw/ (last access: 29 July 2014), 2009. 496
Corripio, J. G.: Snow surface albedo estimation using terrestrial photography, Int. J. Remote Sens., 25, 5705–5729, 2004. 492, 494, 499
Danielson, B. and Sharp, M.: Development and application of a time-lapse photograph analysis method to investigate the link between tidewater glacier flow variations and supraglacial lake drainage events, J. Glaciol., 59, 287–302, 2013. 492
Debella-Gilo, M. and Kääb, A.: Sub-pixel precision image matching for measuring surface displacements on mass movements using normalized cross-correlation, Remote Sens. Environ., 115, 130–142, 2011. 493, 501
Evans, A. N.: Glacier surface motion computation from digital image sequences, IEEE T. Geosci. Remote, 38, 1064–1072, 2000. 493
Fletcher, R.: Modified Marquardt subroutine for non-linear least squares, Tech. Rep. AERE-R–6799, Atomic Energy Research Establishment, Harwell, England, 971. 499
Flotron, A.: Photogrammetirsche Messungen von Gletscherbewegunen mit automatischer Kamera, Schweiz. Z. Vermess. Photogramm. Kult. Tech., 71, 1–73, 1973. 492, 493
Härer, S., Bernhardt, M., Corripio, J. G., and Schulz, K.: PRACTISE – Photo Rectification And ClassificaTIon SoftwarE (V.1.0), Geosci. Model Dev., 6, 837–848, doi:10.5194/gmd-6-837-2013, 2013. 492, 494, 499
Harrison, W. D., Raymond, C. F., and MacKeith, P.: Short period motion events on Variegated Glacier as observed by automatic photography and seismic methods, Ann. Glaciol., 8, 82–89, 1986. 492, 493, 494
Harrision, W. D., Echelmeyer, K. A., Cosgrover, D. M., and Raymond, C. F.: The determination of glacier speed by time-lapse photography under unfavorable conditions, J. Glaciol., 38, 257–265, 1992. 493
Heid, T. and Kääb, A.: Evaluation of existing image matching methods for deriving glacier surface displacements globally from optical satellite imagery, Remote Sens. Environ., 118, 339–355, 2012. 500
Jackson, M., Brown, I. A., and Elvehøy, H.: Velocity measurements on Engabreen, Norway, Ann. Glaciol., 42, 29–34, 2005. 503
Kääb, A.: Monitoring high-mountain terrain deformation from repeated air- and spaceborne optical data: examples using digital aerial imagery and ASTER data, ISPRS J. Photogramm. Remote Sens., 57, 39–52, 2002. 493

GID
4, 491–513, 2014

ImGRAFT: Image GeoRectification And Feature Tracking toolbox

A. Messerli and A. Grinsted

Kääb, A. and Vollmer, M.: Surface geometry, thickness changes and flow fields on creeping mountain permafrost: automatic extraction by digital image analysis, Permafrost Periglac. Process., 11, 315–326, 2000. 493

Messerli, A. and Grinsted, A.: Image GeoRectification And Feature Tracking (ImGRAFT) toolbox main website, http://imgraft.glaciology.net, last access: 14 August 2014. 494, 498, 499, 505

Muslow, C., Koschitzki, R., and Maas, H.-G.: Photogrammetric Monitoring of Glacier Margin Lakes, ISPRS Archives J. Photogramm. Remote Sens. Spatial Inf. Sci., 1, 1–6, 2013. 492

Parajka, J., Haas, P., Kirnbauer, R., Jansa, J., and Blöschl, G.: Potential of time-lapse photography of snow for hydrological purposes at the small catchment scale, Hydrol. Process., 26, 3327–3337, 2012. 492

Smith Jr., K. L., Baldwin, R. J., Glatts, R. C., Chereskin, T. K., Ruhl, H., and Lagun, V.: Weather, ice, and snow conditions at Deception Island, Antarctica: long time-series photographic monitoring, Deep Sea-Res. Pt. II, 50, 1649–1664, 2003. 492

Vogel, C., Bauder, A., and Schindler, K.: Optical Flow for Glacier Motion Estimation, ISPRS Annals J. Photogramm. Remote Sens., 1, 359–364, 2012. 500

Walter, F., O'Neel, S., McNamara, D., Pfeffer, W. T., Bassis, J. N., and Fricker, H. A.: Iceberg calving during transition from grounded to floating ice: Columbia Glacier, Alaska, Geophys. Res. Lett., 10, L15501, doi:10.1029/2010GL043201, 2010. 493

GID

4, 491–513, 2014

ImGRAFT: Image GeoRectification And Feature Tracking toolbox

A. Messerli and A. Grinsted

Table 1. Image pair IDs and parameters used in the error calculation, including the median velocity for Subset 1 (Fig. 4) for each image pair.

Image Pair ID	Date *image A*	Date *image B*	Time	Interval	Median velocity (m day^{-1})
1151a	17 Jul 2013	22 Jul 2013	11:04	5 days	0.54
1252b	17 Jul 2013	22 Jul 2013	14:04	5 days	0.49
1167a	17 Jul 2013	24 Jul 2013	11:04	7 days	0.53
1268b	17 Jul 2013	24 Jul 2013	14:04	7 days	0.51
1175a	17 Jul 2013	25 Jul 2013	11:04	8 days	0.54
1276b	17 Jul 2013	25 Jul 2013	14:04	8 days	0.52
1183a	17 Jul 2013	26 Jul 2013	11:04	9 days	0.53
1284b	17 Jul 2013	26 Jul 2013	14:04	9 days	0.53
1191a	17 Jul 2013	27 Jul 2013	11:04	10 days	0.54
1292b	17 Jul 2013	27 Jul 2013	14:04	10 days	0.52
					Mean: 0.53
					Range: 0.05

GID
4, 491–513, 2014

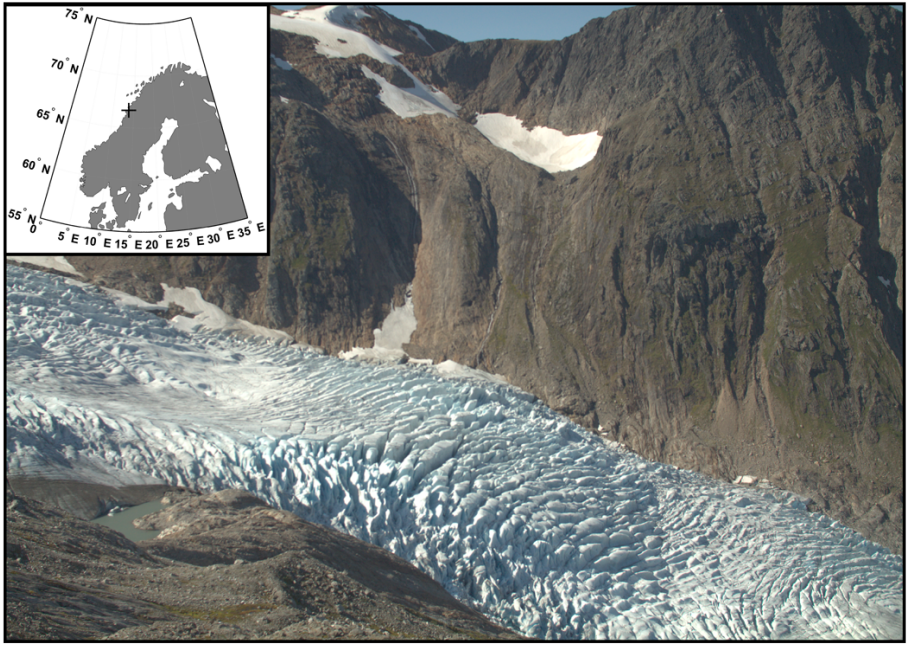

Figure 1. A sample image taken by the time-lapse camera located at Engabreen, northern Norway (inset). Note the distinct crevasse features in the main icefall.

GID
4, 491–513, 2014

ImGRAFT: Image GeoRectification And Feature Tracking toolbox

A. Messerli and A. Grinsted

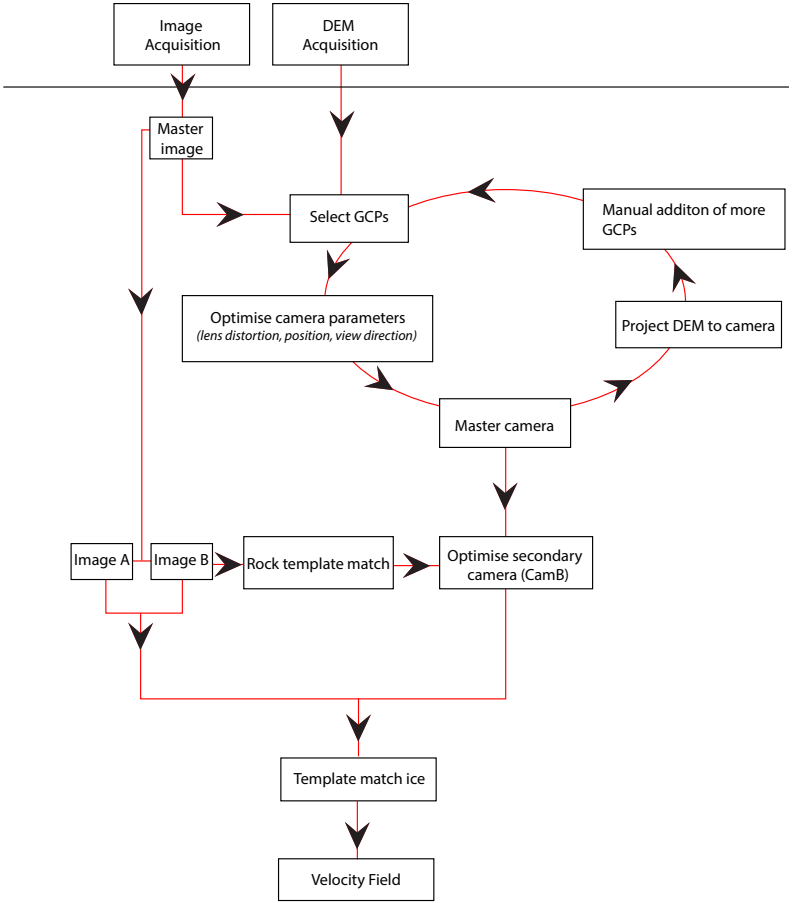

Figure 2. A schematic overview of the key steps in the ImGRAFT processing chain.

GID
4, 491–513, 2014

ImGRAFT: Image GeoRectification And Feature Tracking toolbox

A. Messerli and A. Grinsted

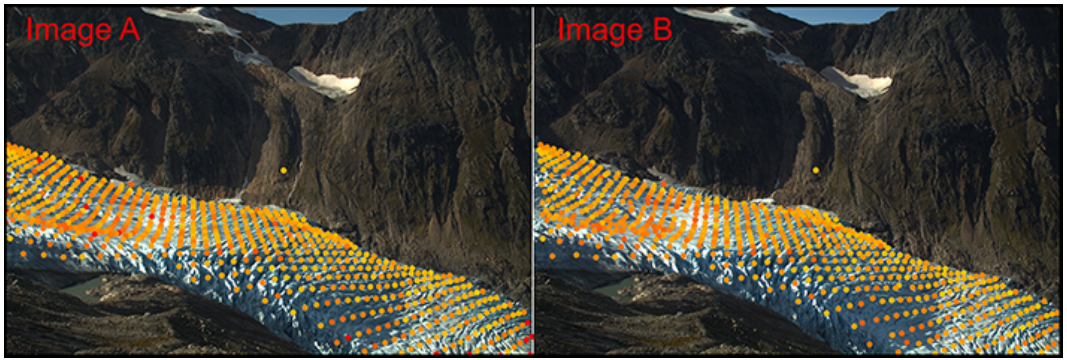

Figure 3. Screen shot of the template matching stage of the processing chain. The regularly spaced grid can be seen in left hand image and the corresponding "tracked" points can be seen in the right hand image. The marker colour corresponds to the quality, yellow indicating a good match between images.

GID
4, 491–513, 2014

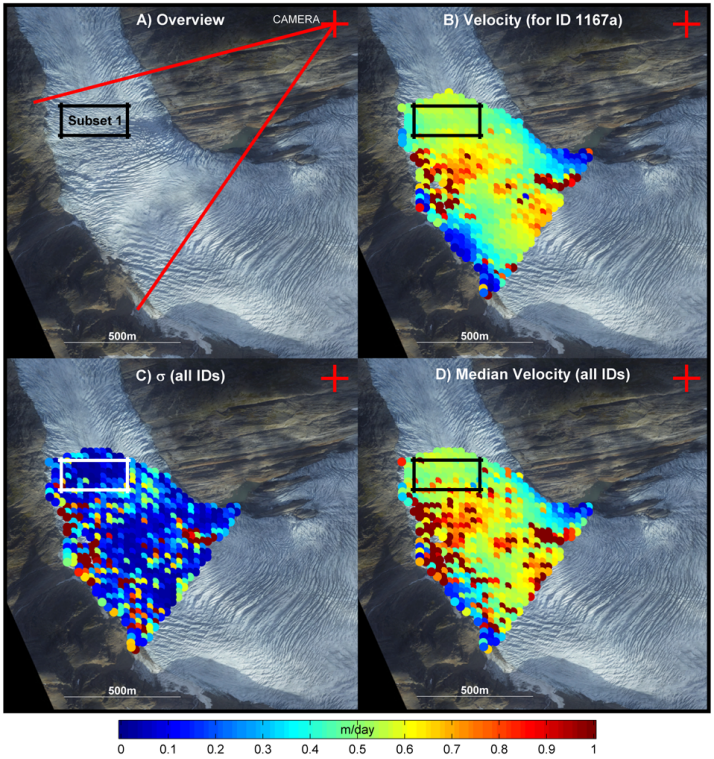

Figure 4. (a) provides an overview of the time-lapse location on the valley side and the red lines indicate the viewshed. Subset 1 is the test area used to derive the median displacements presented in Table 1. **(b)** is an example of the raw velocity field produced as output from the ImGRAFT toolbox. **(c)** is an example standard deviation plot of velocity fields produced from all the image pairs in Table 1. **(d)** is a median velocity plot for all the image pairs presented in Table 1. Note that we use the median over the mean as it is robust to outliers.

GID
4, 491–513, 2014

ImGRAFT: Image GeoRectification And Feature Tracking toolbox

A. Messerli and A. Grinsted